Femtosecond Optical Switching of Electron Transport Direction in Branched Donor−Acceptor Arrays

Aaron S. Lukas, Scott E. Miller, and Michael R. Wasielewski*

Department of Chemistry, Northwestern University, Evanston, Illinois 60208-3113

Received: October 25, 1999

The branched donor−acceptor triad **4** and tetrad **5** were synthesized to study the possibility of controlling the direction of electron transfer in a divergent array of electron acceptors using ultrafast laser pulses. Compounds **4** and **5** employ 1,3,5-triaminobenzene as the central branch point. In **4**, a 4-(*N*-piperidinyl)-1,8-naphthaleneimide electron donor (ANI) was attached to the 1 position and two electron acceptors, 1,8:4,5-naphthalenediimide, NI, and pyromellitimide, PI, were attached to the 3 and 5 positions of the central benzene ring. In **5**, the terminal end of the PI acceptor is functionalized with an additional NI molecule. Selective excitation of ANI in **4** and **5** with 400 nm, 130 fs laser pulses results in exclusive formation of NI^--ANI^+-PI and $NI^-ANI^+-PI-NI$, respectively, with $\tau = 115$ ps, and a quantum yield of 0.99. Excitation of NI^- with 480 nm, 130 fs laser pulses produces the excited doublet state $*NI^-$, which transfers an electron to PI on the second branch of the benzene ring with a time constant of $\tau = 600$ fs in **4** and $\tau = 750$ fs in **5**. The overall quantum yields for the two step process are 0.44 and 0.36 in **4** and **5**, respectively. The resultant state $NI-ANI^+-PI^-$ in **4** undergoes a charge shift reaction returning to the initial ion pair state NI^-ANI^+-PI with $\tau = 400$ ps, while the corresponding state $NI-ANI^+-PI^-NI$ in **5** undergoes a charge shift with $\tau = 200$ ps to yield $NI-ANI^+-PI-NI^-$, which in turn exhibits a 2000 ps lifetime. These results show that once the electron has been switched to the branch containing the thermodynamically uphill PI acceptor, the electron will cascade down that branch to other acceptors that are more easily reduced. Model compounds **1**−**3**, which were synthesized to aid in characterization of the switching dynamics, are also discussed. Photochemical control of directional charge transport may make it possible to design networks of organic molecules for information processing.

Introduction

Branched architectures have been employed for some time in inorganic semiconductors used in optical waveguides and all-optical switching devices.[1,2] However, these systems rely principally on nonlinear optical phenomena and changes in refractive index of the semiconductors to carry out optical switching. In contrast, chemists have focused on the design of isolated complexes and single molecules as potential switching devices. The preparation and study of molecules for use as molecule-sized switching devices is an active area of research.[3−37] Generally, approaches to molecule-sized switches have employed excitation photoisomerization,[10,18,25,30,33−36] energy transfer,[8] electron transfer,[9,16,17,19,20,23,24,27,35,38−41] changes in chirality,[21,29,42] single-molecule photophysics,[22,28,32] photomechanical behavior,[26] and changes in spin state[31] as a means of switching. Only recently have semiconductor design strategies been applied to organic single molecule electronic devices. The fact that many of the properties of bulk electronics do not apply to the molecular regime leads us to explore the fundamental issues that arise at this architectural length scale. One of these issues involves controlling the flow of electrons through branch points between molecules, which is a necessary prerequisite for the design of networks. The wide versatility of organic electron transfer systems makes them excellent candidates for these studies. Energy and electron transfer processes within single molecules can occur on the femtosecond time scale. Thus, it may be possible to use them to construct molecular analogues of electronic devices that respond equally rapidly.

Previous work in our laboratory has demonstrated the ability to control the populations of radical ion intermediates within a linear donor−acceptor(1)−acceptor(2) array using femtosecond laser pulses.[39] In this paper we report one- and two-pulse picosecond electron transfer dynamics in two branched donor−acceptor systems, triad **4** and tetrad **5**, which employ a 1,3,5-triaminobenzene ring as a branch point. Molecules **1**−**3** serve as reference compounds that aid in the elucidation of the electron transfer processes within **4** and **5**. Excitation of the 4-(*N*-piperidinyl)naphthalene-1,8-imide (ANI) electron donor with an initial femtosecond laser pulse leads to selective one-electron reduction of the 1,8:4,5-naphthalenediimide (NI) acceptor, which forms one of the branches. Subsequent selective excitation of the corresponding radical anion, NI^- with a second femtosecond laser pulse results in electron transfer from $*NI^-$ to the pyromellitimide (PI) acceptor on the adjacent branch. Thus, switching of the charge separated ion pair from one branch to the other is accomplished by application of the second femtosecond laser pulse. Elaboration of each of these branches with other acceptors that can accept the electron from either NI^- or PI^- via a thermal electron transfer reaction can provide extended pathways for movement of electrons along each of these branches. The electron transfer dynamics of tetrad **5** illustrate this behavior. These results open up the possibility of designing networks of organic molecules in which electron movement

* To whom correspondence should be addressed. E-mail: wasielew@chem.nwu.edu.

10.1021/jp993774e CCC: $19.00
Published on Web 01/12/2000

CHART 1

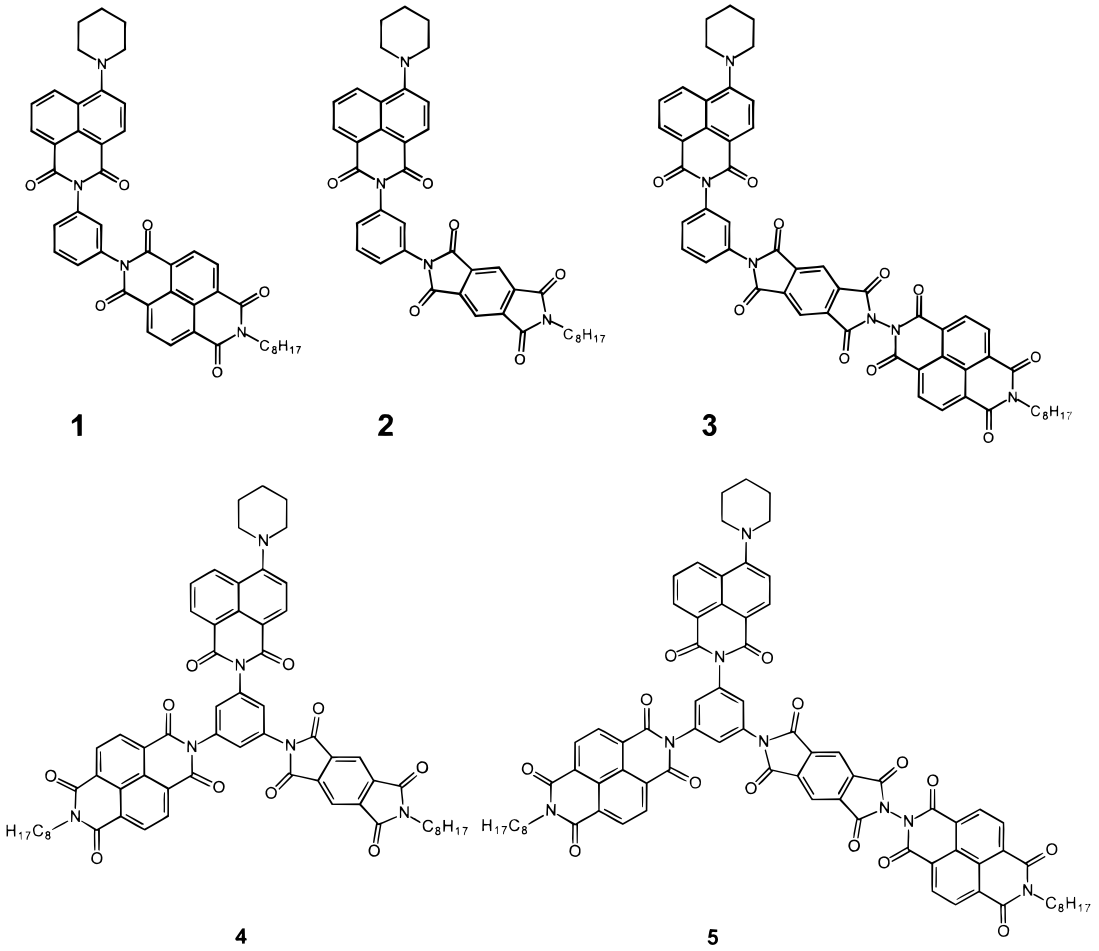

through the network can be controlled by the appropriate sequence of ultrafast laser pulses.

Results and Discussion

Synthesis. The synthesis of compounds **1**−**5** (Chart 1) follows procedures similar to those developed previously[43] and is outlined in Scheme 1. 4-Bromonaphthalene-1,8-dicarboxyanhydride is condensed with a mole of 1,3-phenylenediamine or 1,3,5-triaminobenzene to produce the corresponding 3-aminophenylcarboximide, **6**, or 3,5-diaminophenylcarboximide, **10**. Nucleophilic displacement of the 4-bromo group on the naphthalene in **6** and **10** is carried out using an excess of piperidine to yield the corresponding 4-(*N*-piperidinyl) derivatives, **7** and **11**, respectively. The 4-(*N*-piperidinyl)naphthalene-1,8-dicarboximide serves as the photoexcited electron donor in **1**−**5**. Condensation of **6** with *N*-(*n*-octyl)-naphthalene-1,8-dicarboxyanhydride-4,5-dicarboximide or *N*-(*n*-octyl)-benzene-1,2-dicarboxy-anhydride-4,5-dicarboximide yields the corresponding single-donor−single-acceptor reference compounds **1** or **2**, respectively. The triad reference compound **3** is prepared by condensation of **6** with anhydride **8**, which contains both the PI and NI electron acceptors. Compound **8** is prepared by condensation of the known *N*-amino-*N*′-(*n*-octyl)naphthalene-1,8:4,5-dicarboximide[44] with a mole of pyromellitic dianhydride.

The branched triad and tetrad, **4** and **5**, respectively, use 1,3,5-triaminobenzene, **9**, as the central branch point. Condensation of **9** with one mole of 4-bromonaphthalene-1,8-dicarboxyanhydride yields diamine **10**. Nucleophilic displacement of the 4-bromo group with excess piperidine in NMP yields **11**, which possesses the ANI electron donor and two amines for elaboration of the two electron accepting branches. Reaction of **11** with an excess of of *N*-(*n*-octyl)-naphthalene-1,8-dicarboxyanhydride-4,5-dicarboximide or *N*-(*n*-octyl)-benzene-1,2-dicarboxyanhydride-4,5-dicarboximide yields the single-acceptor monoamines **12** or **13**, respectively. Further reaction of monoamine **13** with an excess of *N*-(*n*-octyl)-naphthalene-1,8-dicarboxyanhydride-4,5-dicarboximide yields triad **4**. Similarly, reaction of monoamine **12** with an excess of anhydride **8** yields tetrad **5**.

Single-Pulse Electron Transfer Dynamics. The photophysics of the 4-(*N*-piperidinyl)naphthalene-1,8-imide (ANI) chromophore have been characterized in detail earlier.[43] Briefly, the ground-state optical spectrum of ANI exhibits a broad absorption at 400 nm, which possesses about 70% charge-transfer character.[38,43] This charge transfer state decays radiatively with an emission maximum at 500 nm in toluene. The fluorescence quantum yield and lifetime of ^{1}*ANI in toluene are 0.91 and 8.5 ns, respectively. ^{1}*ANI readily donates or accepts electrons in the presence of nearby electron acceptors or donors. The one-electron oxidation and reduction potentials of ANI are 1.20 V (vs SCE) and −1.41 V, respectively, while the one-electron reduction potentials of PI and NI are −0.79 V and −0.53 V, respectively. The energy levels of the ion pair states for molecules **1**−**5** were determined using the 2.80 eV energy of ^{1}*ANI, the redox potentials of ANI and the naphthalenediimide (NI) and pyromellitimide (PI) acceptors, as well as the Coulombic interaction energy between ANI^+ and NI^- or PI^- by methods given previously.[43] The energy levels of the ion pair states in molecules **1**−**3** are given in Figure 1, while those for **4** and **5** are presented in Figures 8 and 9.

SCHEME 1

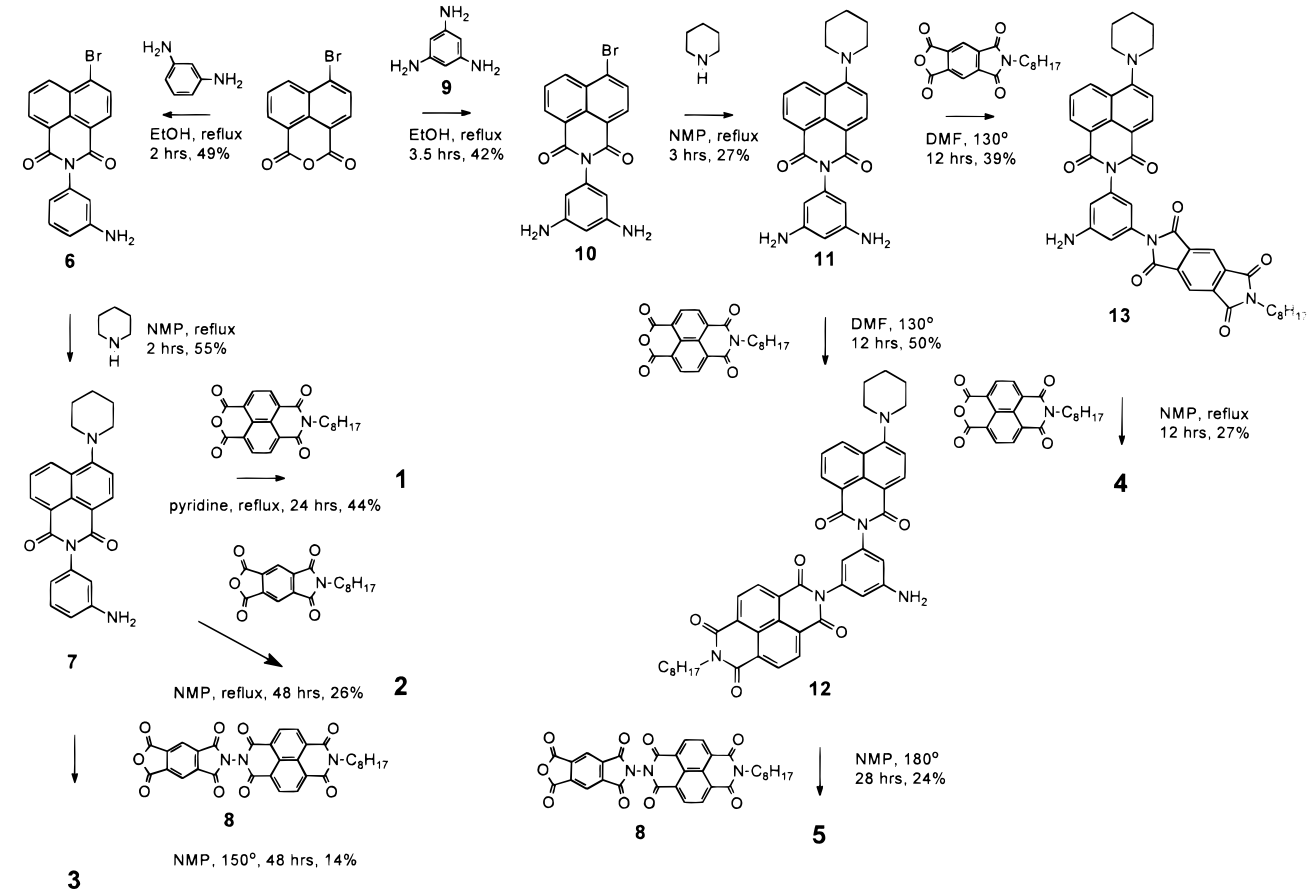

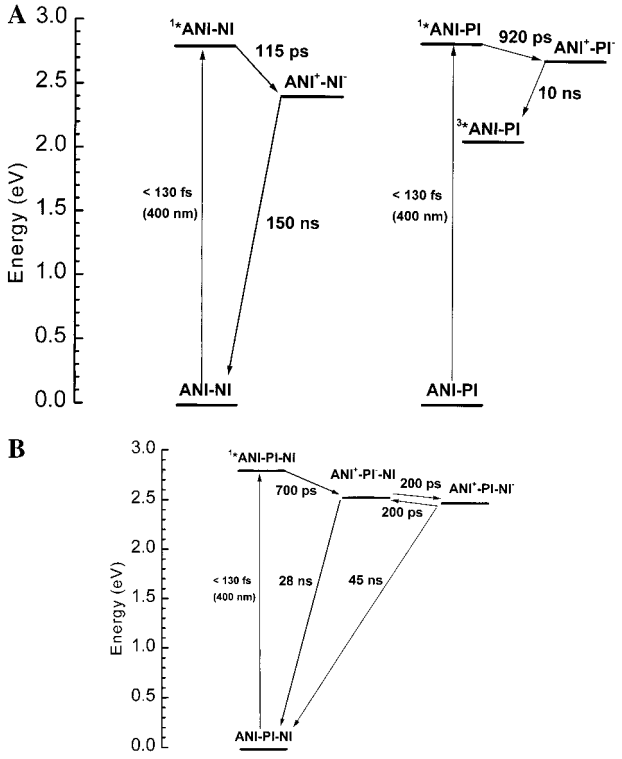

Figure 1. Energy level diagrams for (A) **1** and **2** and (B) **3**, all in toluene.

Transient absorption measurements on **1** and **2** show that direct excitation of the ANI chromophore using 130 fs, 400 nm laser pulses results in electron transfer from ^{1}*ANI to the adjacent NI and PI acceptors. Figure 2 shows the transient

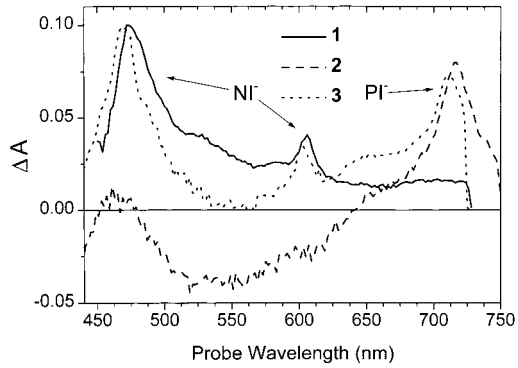

Figure 2. Single pulse transient absorption spectra of **1**−**3** in toluene at $t = 2$ ns after excitation with 400 nm, 130 fs laser pulses. Note that in **3** the spectral signatures of both NI^- and PI^- are present.

spectra of the charge separated states, ANI^+-NI^- in **1** and ANI^+-PI^- in **2**, which exhibit characteristic optical absorptions for NI^- at 480 and 610 nm[45] and for PI^- at 720 nm.[46] The transient kinetics in Figure 3 show that ANI^+-NI^- in **1** and ANI^+-PI^- in **2**, form with $\tau = 115$ ps and $\tau = 920$ ps, respectively. This suggests that electron transfer constitutes the major deactivation pathway competing with fluorescence from ^{1}*ANI, and that based on the 8.5 ns lifetime of ^{1}*ANI, the quantum yield for production of ANI^+-NI^- in **1** is 0.99, while that for ANI^+-PI^- in **2** is 0.90. Charge recombination of ANI^+-NI^- within **1** occurs with a time constant of $\tau = 150$ ns and $\Delta G = -2.4$ eV to produce the ground state of **1**, while recombination of ANI^+-PI^- within **2** occurs with a time constant of $\tau = 10$ ns and $\Delta G = -0.6$ eV to produce primarily ^{3}*ANI. The free energy of the reaction $ANI^+-NI^- \rightarrow ANI-NI$ lies strongly in the Marcus inverted region[47] and is thus

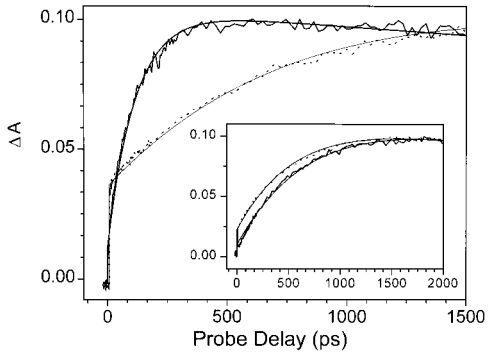

Figure 3. Transient absorption kinetics for **1** (—) at 480 nm and **2** (– –) at 720 nm in toluene following excitation with a single 400 nm, 130 fs, laser pulse. Inset: transient absorption kinetics for **3** at 480 nm (—) and 720 nm (– –) in toluene following excitation with a single 400 nm, 130 fs laser pulse. Nonlinear least-squares fits to the data are also shown.

substantially slower than the reaction $ANI^+-PI^- \rightarrow {}^3*ANI-PI$, which lies in the normal region.

When an N–N bond is used to directly link PI and NI, the one-electron reduction potential of PI is shifted more positive by approximately 0.1V.[48] This makes the free energy for charge separation to PI 0.1 eV more negative. Thus, direct attachment of NI to PI in **3** results in a somewhat faster charge separation reaction $^1*ANI-PI-NI \rightarrow ANI^+-PI^--NI$ with $\tau = 700$ ps. The yield of ANI^+-PI^--NI likewise increases to 0.92. The time constant for the charge shift reaction $ANI^+-PI^--NI \rightarrow ANI^+-PI-NI^-$ is $\tau = 200$ ps. The transient absorption spectrum of the charge separated intermediate within **3** is shown in Figure 2, while the kinetics for charge separation detected at 480 and 720 nm are shown in the inset to Figure 3. The overall yield for the two step charge separation is also 0.92, as the charge recombination reaction $ANI^+-PI^--NI \rightarrow {}^3*ANI-PI-NI$ with $\tau = 10$ ns cannot compete kinetically with charge separation to NI. However, the transient absorption spectrum of **3** shown in Figure 2 indicates that PI^- and NI^- are in equilibrium. While NI is 0.26 V easier to reduce than is PI, in low polarity media such as toluene, the additional Coulombic energy required to move the positive and negative charges further apart in the reaction $ANI^+-PI^--NI \rightarrow ANI^+-PI-NI^-$ cancels most of the redox potential difference between PI and NI that thermodynamically favors the formation of $ANI^+-PI-NI^-$. Calculations using the spectroscopic/electrochemical method of Greenfield et al. show that the $ANI^+-PI-NI^-$ state lies approximately 0.08 eV below that of ANI^+-PI^--NI.[43] Thus, these ion pair states are effectively isoenergetic. The similarity between the 28 ns and 45 ns time constants for charge recombination of $ANI-PI^--NI$ and $ANI-PI-NI^-$ within **3** suggests that significant populations of both PI^- and NI^- are present during the charge recombination process.

In the molecular switch prototypes, **4** and **5**, the donor and acceptor groups are spaced evenly about the phenyl junction. Molecular mechanics calculations yield structures for **4** and **5**, Figure 4, which show that steric interactions result in similar, substantial dihedral angles between the π systems of ANI, NI, and PI relative to that of the trisubstituted benzene, as well as between the PI directly bonded to NI within **5**.[49] These strong deviations from an all planar structure substantially reduce the electronic coupling between the various electron donors and acceptors within **4** and **5**. Distances of approximately 14 Å and four similar chemical bonds separate the ANI electron donor from either the NI or PI acceptors attached to the benzene branch point.[49] Thus, the electronic coupling between the donor and each acceptor should be similar, and the electron transfer rates from $^1*ANI$ to either PI or NI in these systems should be determined primarily by their free energies of reaction. Electron transfer from $^1*ANI$ to NI is energetically favored over that to PI by approximately 0.26 eV. Consequently, excitation of ANI in **4** and **5** with 400 nm laser pulses results exclusively in formation of ANI^+-NI^- with $\tau = 115$ ps and a quantum yield of 0.99. The charge separation time constants and the yields of the NI^--ANI^+-PI and $NI^--ANI^+-PI-NI$ ion pair states in **4** and **5**, respectively, are identical to those observed for compound **1**. There is no spectral evidence for electron transfer to PI in either molecule, as seen in the inset to Figure 5. The

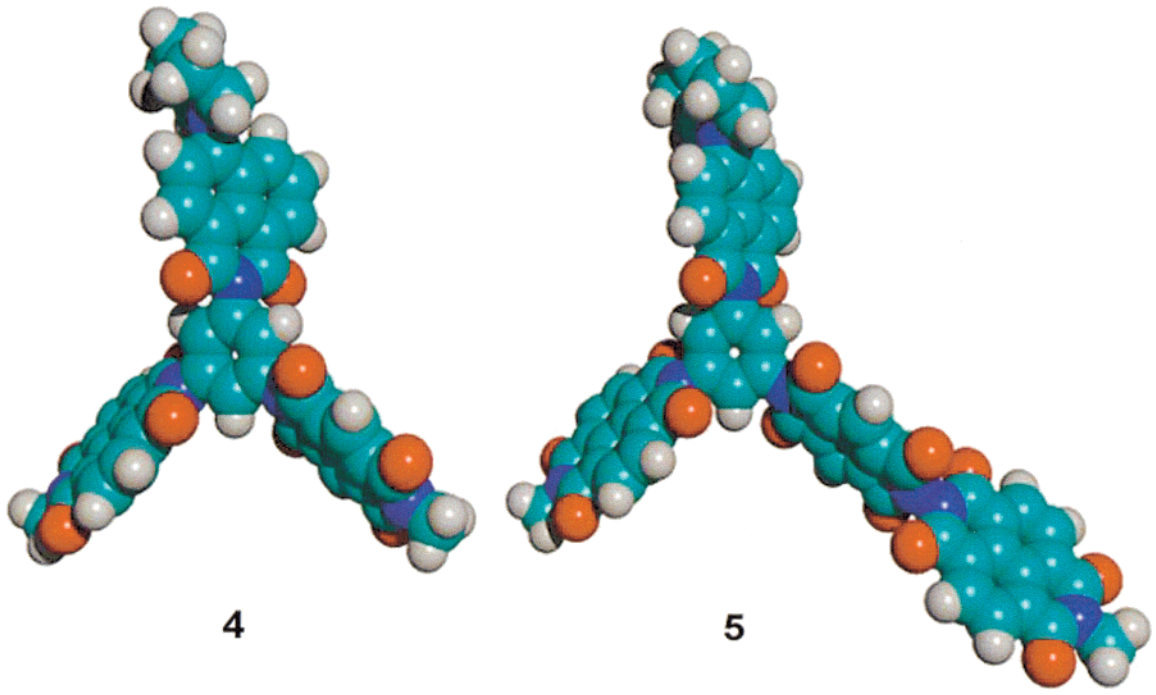

Figure 4. Structures of **4** and **5** derived from molecular mechanics calculations.

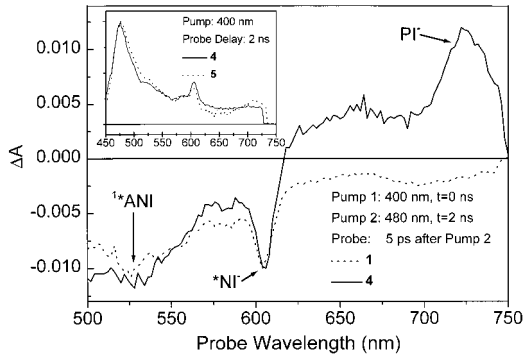

Figure 5. Two pump transient absorption spectra of **1** and **4** in toluene. Inset: single pulse transient absorption spectra of **4** and **5** at $t = 2$ ns after excitation with 400 nm, 130 fs laser pulses.

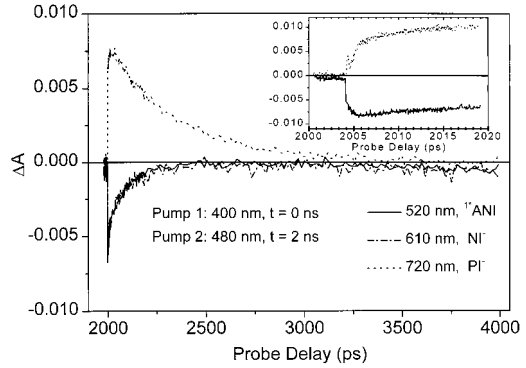

Figure 6. Two pulse transient absorption kinetics for **4**. Inset: The formation of ^{1}*ANI at 525 nm (—), and PI^- at 720 nm (– –) in compound **4**.

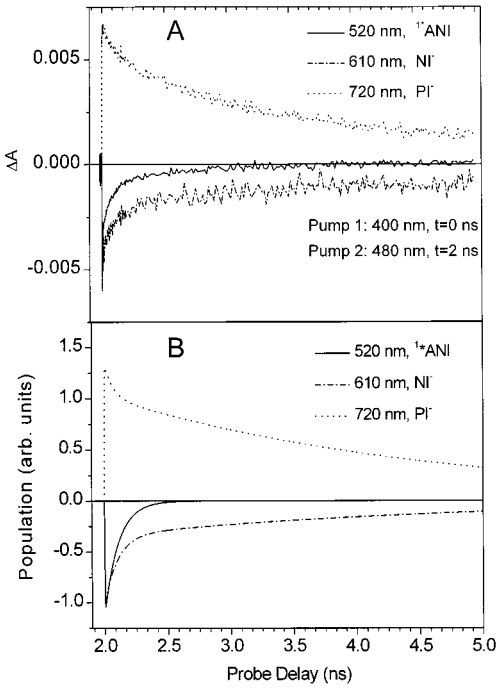

Figure 7. (A) Two pulse transient absorption kinetics for **5**. (B) Kinetic modeling for compound **5** as discussed in the text.

charge recombination reactions of NI^-–ANI^+–PI and NI^-–ANI^+–PI–NI occur with $\tau = 150$ ns, and once again agree very well with that determined for **1**. Thus, using a single 400 nm excitation pulse, both **4** and **5** exhibit exclusive transfer of an electron to the branch that contains the NI acceptor alone.

Two Pulse Electron Transfer Dynamics. Photoexcitation of radical ions leads to the formation of excited doublet states

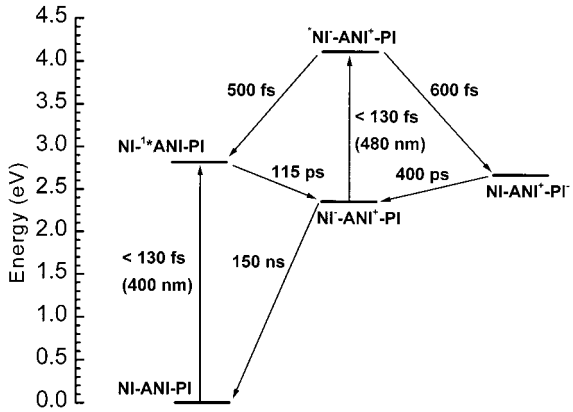

Figure 8. Energy level diagram for compound **4** in toluene.

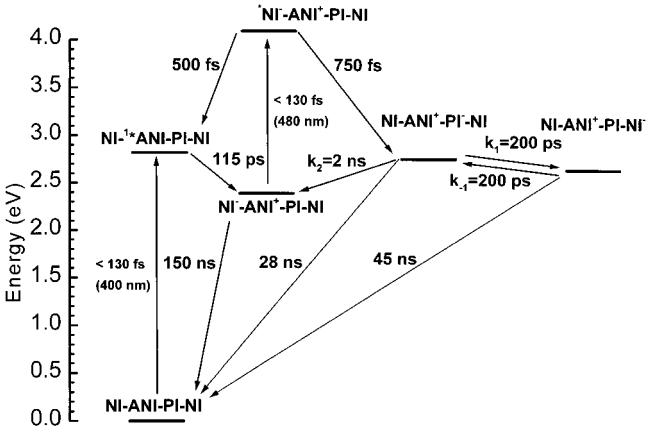

Figure 9. Energy level diagram for compound **5** in toluene.

that may transfer an electron to nearby electron acceptors or to solvent.[50–60] The distinct 480 nm absorption band of NI^- allows for its selective excitation to its lowest excited state *NI^- from which deactivation occurs via competing routes. Excitation of **1** in toluene with a 400 nm laser pulse at $t = 0$ ns initiates the formation of ANI^+–NI^- ($\tau = 115$ ps) as in the single-pulse experiment. Excitation of NI^- with a 480 nm laser pulse at $t = 2$ ns following the 400 nm pulse yields the excited radical anion, ANI^+–*NI^-. Depletion of the NI^- ground state occurs within the 180 fs instrument function, and is observed as a bleach at 610 nm.[39] Deactivation of *NI^- occurs rapidly via charge recombination, reforming ^{1}*ANI–NI with $\tau = 500$ fs. This is indicated by the appearance of the ^{1}*ANI stimulated emission near 525 nm, Figure 5. There is no spectroscopic evidence for charge transfer to nearby solvent molecules. The population of ^{1}*ANI–NI formed via the reaction ANI^+–*NI^- → ^{1}*ANI–NI subsequently reacts to yield the charge separated state, ANI^+–NI^-, again with $\tau = 115$ ps, monitored by the decays of the bleaches at 525 and 610 nm. The data are consistent with a quantum yield near unity for the reaction ANI^+–*NI^- → ^{1}*ANI–NI because the lifetime of *NI^- itself is 240 ps.[61]

Excitation of the branched molecule **4** with a single 400 nm, 130 fs laser pulse at $t = 0$ produces NI–^{1}*ANI–PI, which undergoes electron transfer to yield NI^-–ANI^+–PI. The formation and decay of this ion pair state occurs with the same kinetics observed in **1**. Subsequent excitation of NI^- within NI^-–ANI^+–PI with 480 nm, 130 fs laser pulses at $t = 2$ ns results in the appearance of both the 525 nm stimulated emission band from ^{1}*ANI and the absorption band at 720 nm due to PI^-, Figure 5. This indicates that *NI^-–ANI^+–PI undergoes deactivation via two competitive pathways. *NI^-–ANI^+–PI undergoes charge recombination back to the NI–^{1}*ANI–PI

excited state similar to the dynamics in dyad **1**, or a charge shift to form NI−ANI$^+$−PI$^-$. While the calculated energy levels of the NI−^{1}*ANI−PI and NI−ANI$^+$−PI$^-$ states are similar, Figure 8, the electronic coupling between each of them and *NI$^-$−ANI$^+$−PI may be different. Nevertheless, the observed rates of these competing reactions are similar. The inset to Figure 6 shows that biexponential kinetics are observed for the reactions *NI$^-$−ANI$^+$−PI → NI−^{1}*ANI−PI and *NI$^-$−ANI$^+$−PI → NI−ANI$^+$−PI$^-$. For the charge shift reaction the major kinetic component occurs with $\tau = 600$ fs, while a smaller amplitude $\tau = 6$ ps component also appears. The fast component is assigned to the electron transfer reaction, while the second minor component may be due to either solvent or vibrational relaxation processes.[48] The free energy for each reaction is approximately 1.2 eV, and is near the top of the Marcus parabola (vide infra).[47] Thus, the large driving forces for these reactions are most likely responsible for their ultrafast rates. Small differences in electronic coupling between the reactant and product states involved in the two deactivation pathways most likely have a minor effect on the observed rates. The quantum yield for the charge shift reaction *NI$^-$−ANI$^+$−PI → NI−ANI$^+$−PI$^-$ calculated using the measured rate constants for the two competing deactivation routes is 0.45. Given a 0.99 quantum yield for the formation of NI$^-$−ANI$^+$−PI, the overall quantum yield of NI−ANI$^+$−PI$^-$ formation is 0.44.

The subsequent decay of PI$^-$ within NI−ANI$^+$−PI$^-$ can occur via two possible routes: charge shift back NI, or direct charge recombination with ANI$^+$. Charge recombination within NI−ANI$^+$−PI$^-$ should occur in $\tau = 10$ ns by analogy with **2**. Thus, the observed decay of $\tau = 400$ ps is due entirely to charge shift to NI. The population of the NI$^-$−ANI$^+$−PI state prior to the switching event induced by the second laser pulse is fully restored, as evidenced by the complete recovery of the 610 nm signal to base line, Figure 6.

The structure of compound **5** is very similar to **4** except that a second NI has been directly linked to PI through an N−N bond. As discussed for compound **3**, this stabilizes PI$^-$ by approximately 0.1 V and significantly affects the switching dynamics. The time constant for the reaction *NI$^-$−ANI$^+$−PI−NI → NI−ANI$^+$−PI$^-$−NI increases to $\tau = 750$ fs, and the overall yield of the charge-transfer process also decreases to 0.36. These data suggest that the deactivation of *NI$^-$ is actually slightly in the Marcus inverted region, as an increase in the driving force decreases the reaction rate somewhat. The transient absorption kinetics at 525, 610, and 720 nm for compound **5**, are shown in Figure 7A. In compound **5** both the 610 and 720 nm transient absorption changes display biexponential kinetics. The kinetic analysis is further complicated by the inability to distinguish between the spectra of the two NI$^-$ ion containing intermediates. Comparing the electron transfer pathways detailed in Figures 8 and 9, while a single process determines the lifetime of the NI−ANI$^+$−PI$^-$ ion pair in compound **4**, there are now two possible routes for the decay of NI−ANI$^+$−PI$^-$−NI in **5**. The dynamics are governed by the rate constants labeled k_1, k_{-1}, and k_2 in Figure 9. The rate constant k_1 is known to be (200 ps)$^{-1}$ from the single pulse studies on **3**. However, the rate constants k_{-1}, and k_2 cannot be determined directly. Therefore, kinetic simulations were performed to estimate k_{-1} and k_2.[62] The rate constant k_2 for charge shift from the PI$^-$ containing branch back to the branch with NI alone is likely to decrease from compound **4** to **5** because the free energy of reaction for the charge-transfer back to the first branch decreases. The results are shown in Figure 7B. Biexponential kinetics are observed at 720 nm: an initial fast decay with a time constant of $\tau = 225$ ps, after which the dynamics switch over to a much slower process having a time constant of $\tau = 2200$ ps. The amplitudes for the two components are 1:2, respectively, and are dependent upon the equilibrium constant determined by k_1 and k_{-1}. A steady-state ensues upon establishment of the equilibrium between NI−ANI$^+$−PI$^-$−NI and NI−ANI$^+$−PI−NI$^-$ with the kinetics at longer times determined by k_2. The same argument can be applied to the kinetics observed at 610 nm. However, the amplitude of the fast decay component increases relative to that of the slower process to approximately 2:1, respectively. This can be attributed to the additional rate constant for the forward electron transfer reaction NI−^{1}*ANI−PI−NI → NI$^-$−ANI$^+$−PI−NI, which contributes to the fast kinetics. The best simulation of the experimentally observed decay kinetics for the 610 and 720 nm signals is obtained with $k_1 = 5.0 \times 10^9$ s^{-1} ($\tau = 200$ ps) and $k_2 = 5 \times 10^8$ s^{-1} ($\tau = 2$ ns). The 28 ns and 45 ns time constants for the return of NI−ANI$^+$−PI$^-$−NI and NI−ANI−PI−NI$^-$, respectively, to ground state indicated in Figure 9 are assumed to be the same as the those for the corresponding processes within **3**. Thus, the results show that extension of the number of electron acceptors forming an energetically downhill electron transfer cascade can result in movement of the electron away from the branch point. Further adjustments to both the free energies of reaction and the electronic coupling between the donor and acceptors within these branched molecular switches will be needed to optimize the quantum yields for electron transfer down the branch accessed using the second laser pulse. For example, changing the excited-state energy of the electron donor group is one way to accomplish this. We are thus studying alternatives to ANI as the electron donor.

Summary and Conclusions

These experiments demonstrate that it is possible to control the direction of electron flow within a branched donor−acceptor array on the femtosecond time scale. In triad **4**, the initial ion pair forms over a distance of 14 Å with a quantum yield of 0.99. Excitation of the reduced acceptor group switches the system over to the second ion pair with a yield of 44% in toluene. The second state of the switch decays back to the initial ion pair state and has a lifetime of 400 ps. While the yield of the switching decreases in tetrad **5** to 36%, the kinetic evidence suggests that the lifetime of second state of the switch is increased by about an order of magnitude.

The study of molecular arrays is paramount to developing a fundamental understanding of the stepwise electron transfer processes, which someday may prove useful for processing data. While these studies are most easily done in a fluid solvent, future studies must eventually adapt these concepts to the solid state and to surfaces, where the electron transfer dynamics may differ from those observed in solution. In addition, future research will emphasize improving the yields for switching the ion pairs, extension of the electron transfer pathways along each branch, and strategies for the development of electron transfer networks based on photon controlled branching.

Experimental Section

Syntheses. Proton nuclear magnetic resonance spectra were recorded on a Gemini-300 NMR spectrometer using TMS as an internal standard. Laser desorption mass spectra were obtained with a Kratos MALDI III spectrometer using 2-hydroxy-1-naphthoic acid as a matrix. All solvents and regents were used as received. Column chromatography was performed using Merck silica gel 60.

***N*-(3-aminophenyl)-4-bromonaphthalene-1,8-dicarboximide, 6.** 4-Bromonaphthalene-1,8-dicarboxylic anhydride (5.0 g, 0.018 mol) was dissolved in 300 mL 95% ethanol. 1,3-Phenylenediamine (2.0 g, 0.0185 mol) was added and the solution was bubbled with nitrogen for 10 min. The resulting solution was refluxed for 2 h, cooled to 0 °C for 24 h, and then filtered on a Büchner funnel. The powder was rinsed with ethanol, and dried to yield **6**, 3.22 g, 49%. $C_{18}H_{11}N_2O_2Br$: mass spectrum (*m*/*e*) 368.3 (calcd 367.2), ^{1}H NMR (δ in $CDCl_3$) 8.69 (d, J = 7.2 Hz, 1H, 8-naphthyl), 8.625 (d, J = 8.55 Hz, 1H, 6-naphthyl), 8.45 (d, J = 7.85 Hz, 1H, 2-naphthyl), 8.073 (d, J = 7.85 Hz, 1H, 3-naphthyl), 7.88 (d of d, J = 8.5 Hz, J = 7.3 Hz, 1H, 7-naphthyl), 7.324 (t, J = 7.9 Hz, 1H, 5-phenyl), 6.88 (d, J = 8.1 Hz, 1H, 6-phenyl), 6.69 (d, J = 7.78 Hz, 1H, 4-phenyl), 6.616 (m, 1H, 2-phenyl), 1.9 (broad singlet, 2H, 3-phenylamine).

***N*-(3-aminophenyl)-4-(*N*-piperidyl)naphthalene-1,8-dicarboximide, 7.** Compound **6** (1.0 g, 2.7 mmol) was dissolved in 50 mL of *N*-methylpyrrolidinone (NMP) along with piperidine (2.3 g, 0.027 mol). The solution was refluxed for 2 h under a nitrogen atmosphere. The solvent was stripped on a roughing pump, and the resulting residue was purified using silica gel chromatography. Elution with 10% acetone in methylene chloride v/v, yielded **7** as a yellow powder, 0.55 g, 55%. $C_{23}H_{21}N_3O_2$. Mass spectrum (*m*/*e*) 371.6 (calcd 371.4), ^{1}H NMR (δ in $CDCl_3$) 8.598 (d, J = 7.28 Hz, 1H, 8-naphthyl), 8.522 (d, J = 8.18 Hz, 2-naphthyl), 8.425 (d, J = 8.5 Hz, 1H, 6-naphthyl), 7.692 (d of d, J = 8.46 Hz, J = 8.44 Hz, 1H, 7-naphthyl), 7.30 (t, J = 7.94 Hz, 1H, 5-phenyl), 7.194 (d, J = 8.13 Hz, 1H, 3-naphthyl), 6.76 (d, J = 7.8 Hz, 1H, 6-phenyl), 6.682 (d, J = 7.8 Hz, 1H, 4-phenyl), 6.608 (t, J = 2.0 Hz, 1H, 2-phenyl), 3.78 (broad singlet, 2H, phenylamine), 3.25 (m, 4H, piperidine), 1.88 (m, 4H, piperidine), 1.71 (m, 2H, piperidine).

Compound 1. Compound **7** (0.06 g, 0.162 mmol) was dissolved in 20 mL of pyridine. *N*-(*n*-octyl)-naphthalene-1,8-dicarboxyanhydride-4,5-dicarboximide[43] (0.064 g 0.169 mmol) was added, and the solution was refluxed for 24 h under a nitrogen atmosphere. The pyridine was stripped on a rotary evaporator and the residue was purified using silica gel chromatography. Elution with 5% acetone in methylene chloride v/v yielded **1** as a yellow powder, 0.052 g, 43.8%. $C_{45}H_{40}N_4O_6$: mass spectrum (*m*/*e*) 731.5 (calcd 732.8), ^{1}H NMR (δ in $CDCl_3$) 8.807 (d, J = 3.3 Hz, 4H, naphthalene ring), 8.625 (d, J = 9.0 Hz, 1H, 8-naphthyl), 8.551 (d, J = 8.1 Hz, 1H, 2-naphthyl), 8.431 (d, J = 5.7 Hz,1H, 6-naphthyl), 7.72 (m, 2H, 7-naphthyl, 5-phenyl), 7.485 (m, 2H, 4-phenyl, 6-phenyl), 7.372 (s, 1H, 2-phenyl), 7.204 (d, J = 8.4 Hz, 1H, 3-naphthyl), 4.2 (t, 2H, *N*-methylene), 3.26 (m, 4H, piperidine), 1.9 (m, 4H, piperidine), 1.75 (m, 2H, piperidine), 1.28 (broad singlet, 12H, octyl tail), 0.88 (t, J = 6.6 Hz, 3H, octyl tail methyl).

Compound 2. Compound **7** (0.103 g, 0.028 mmol) was dissolved in 25 mL of NMP along with *N*-(*n*-octyl)-benzene-1,2-dicarboxyanhydride-4,5-dicarboximide (0.214 g, 0.65 mmol). The solution was refluxed for 48 h under a nitrogen atmosphere. The solvent was stripped using a roughing pump. The residue was dissolved in methylene chloride and applied to a silica gel column. Elution with 4% acetone in methylene chloride v/v yielded **2** as a yellow powder, 0.05 g, 26.4%. $C_{41}H_{38}N_4O_6$: mass spectrum 682.6 (calcd 682.8), ^{1}H NMR (δ in $CDCl_3$) 8.62 (d, J = 7.32 Hz, 1H, 8-naphthyl), 8.545 (d, J = 8.13 Hz, 1H, 2-naphthyl), 8.452 (d, J = 8.44 Hz, 1H, 6-naphthyl), 8.367 (s, 2H, pyromellitimide), 7.715 (d of d, J = 8.4 Hz, J = 7.3 Hz, 1H, 7-naphthyl), 7.68 (m, 2H, 4-phenyl, 6-phenyl), 7.592 (t, J = 1.5 Hz, 1H, 2-phenyl), 7.4 (m, 1H, 5-phenyl), 7.215 (d, J = 8.05 Hz, 1H, 3-naphthyl), 3.75 (t, J = 7.3 Hz, 2H, *N*-methylene), 3.28 (m, 4H, piperidine), 1.9 (m, 4H, piperidine), 1.74 (m, 2H, piperidine), 1.25 (broad singlet, 12H, octyl tail), 0.87 (t, J = 6.3 Hz, 3H, octyl tail methyl).

***N*-octyl-*N*′-(*N*′′-(1,2-Dicarboximide)-4,5-dicarboxyanhydride)-naphthalene-1,2:4,5-dicarboximide, 8.** Pyromellitic dianhydride (1.0 g, 9.2 mmol) and *N*-amino-*N*′-octylnaphthalene-1,8:4,5-dicarboximide[44] (0.755 g, 1.92 mmol) were dissolved in 15 mL of DMF and heated to 140° for 24 h under a nitrogen atmosphere. The solvent was stripped and the residue was purified using silica gel chromatography. Elution with 10% methanol in methylene chloride resulted in **8** as a sticky solid, 0.955 g, 85% yield. $C_{32}H_{23}N_3O_8$: no mass spectrum available. ^{1}H NMR (δ in DMSO) 8.786 (s, 4H, naphthalene diimide), 8.475 (s, 2H, pyromellitc monoanhydride mono-imide), 4.06 (m, 2H, *N*-methylene), 1.676 (m, 2H, octyl tail), 1.26 (broad singlet, 10H, octyl tail), 0.859 (t, J = 6.3 Hz, 3H, octyl tail methyl).

Compound 3. Compounds **7** (0.060 g, 0.16 mmol) and **8** (0.224 g, 0.387 mmol) were dissolved in 10 mL of NMP and heated at 150° for 48 h under a nitrogen atmosphere. This solution was cooled, taken up in 30 mL of chloroform, and washed with water (3 × 1000 mL). The organic layer was dried over anhydrous magnesium sulfate, and stripped of solvent. The residue was then adsorbed onto silica gel and purified using silica gel chromatography. The product was eluted with 5% acetone in methylene chloride (v/v), and the solvent stripped to yield **3** as a yellow powder, 52 mg, 14%. $C_{55}H_{42}N_6O_{10}$: mass spectrum 947.5 (calcd 947.0), ^{1}H NMR (δ in $CDCl_3$) 8.85 (s, 4H, naphthalene ring), 8.63 (d, J = 7.32 Hz, 1H, 8-naphthyl), 8.56 (d, J = 8.09 Hz, 1H, 2-naphthyl), 8.56 (s, 2H, pyromellitimide ring), 8.46 (d, J = 8.5 Hz, 1H, 6-naphthyl), 7.72 (m, 3H, 7-naphthyl, 6-phenyl, 4-phenyl), 7.63 (m, 1H, 2-phenyl), 7.45 (m, 1H, 5-phenyl), 7.22 (d, J = 8.26 Hz, 1H, 3-naphthyl), 4.23 (t, J = 7.57 Hz, 2H, *N*-methylene), 3.275 (m, 4H, piperidine ring), 1.92 (m, 4H, piperidine ring), 1.76 (m, 2H, piperidine ring), 1.25 (broad singlet, 12H, octyl tail), 0.89 (t, J = 7.0 Hz, octyl tail methyl).

1,3,5-Triaminobenzene, 9. 3,5-Dinitroaniline (1.592 g, 8.7 mmol) was dissolved in 50 mL of ethanol along with 1.5 g 5% Pd on activated carbon. This solution was deoxygenated by bubbling with nitrogen and heated to reflux. Hydrazine monohydrate (2.06 g, 41.2 mmol) was added dropwise to the refluxing solution. The reaction was heated an additional 15 min, then filtered through Celite 454. The product was eluted from the Celite using 150 mL of methanol. The product and the unreacted hydrazine monohydrate were codistilled with 20 mL of DMF on a rotary evaporator. The sticky black product was used immediately without further characterization to avoid rapid decomposition.

***N*-(3,5-Diaminophenyl)-4-bromonaphthalene-1,8-dicarboximide, 10.** Compound **9** (1.07 g, 8.7 mmol) was dissolved in 150 mL of ethanol. 4-Bromo-1,8-naphthalic dianhydride (1.5 g, 5.4 mmol) was added, and the solution was refluxed under nitrogen for 3.5 h. The reaction was then cooled to 0 °C for at least 4 h and filtered using a Büchner funnel. The crude product was adsorbed onto silica gel using methylene chloride and eluted from a silica gel column using 50% acetone in methylene chloride v/v. The solvent was stripped to yield **10**, 0.867 g, 42%. $C_{18}H_{12}N_3O_2Br$: mass spectrum 348.3 (calcd 348.3), ^{1}H NMR (δ in DMSO) 8.61 (d, J = 7.47 Hz, 1H, 6-naphthyl), 8.584 (d, J = 8.56 Hz, 1H, 8-naphthyl), 8.373 (d, J = 7.85 Hz, 1H, 3-naphthyl), 8.251 (d, J = 7.89 Hz, 1H, 2-naphthyl), 8.025 (d of d, J = 7.37 Hz, J = 7.29 Hz, 1H, 7-naphthyl), 5.89 (s, 1H,

4-phenyl), 5.72 (s, 2H, 2,6-phenyl), 3.48 (broad singlet, 4H, 3,5-phenylamine).

***N*-(3,5-Diaminophenyl)-4-(*N*-piperidyl)-naphthalene-1,8-dicarboximide, 11.** Compound **10** (1.8 g (4.7 mmol) and piperidine (2.9 g, 34 mmol) were dissolved in 50 mL of NMP and refluxed 3−4 h under a nitrogen atmosphere. The solvent was removed using a roughing pump, and the sticky residue was taken up in a minimum amount of methylene chloride. The dissolved residue was added dropwise to 50 mL of petroleum ether and centrifuged 15 min. The powdery precipitate was purified using silica gel column chromatography, eluting with 10% acetone in methylene chloride to yield **11** as a yellow powder, 0.482 g, 26.5%. $C_{23}H_{22}N_4O_2$: mass spectrum (*m*/*e*) 387.4 (calcd 386.5), ^{1}H NMR (δ in $CDCl_3$) 8.604 (d, $J = 6.69$ Hz, 1H, 8-naphthyl), 8.528 (d, $J = 8.1$ Hz, 1H, 2-naphthyl), 8.426 (d, $J = 8.5$ Hz, 1H, 6-naphthyl), 7.695 (d of d, $J = 7.31$ Hz, $J = 8.42$ Hz, 1H, 7-naphthyl), 7.197 (d, $J = 8.22$ Hz, 1H, 3-naphthyl), 6.10 (m, 1H, 4-phenyl), 6.06 (m, 2H, 2-phenyl, 6-phenyl), 3.67 (broad singlet, 4H, 3,5-phenylamines), 3.242 (m, 4H, piperidine), 1.90 (m, 4H, piperidine), 1.73 (m, 2H, piperidine).

Compound 12. Compound **11** (0.116 g, 0.297 mmol) was dissolved in 15 mL of DMF and heated to 130°. *N*-(*n*-octyl)-naphthalene-1,8-dicarboxyanhydride-4,5-dicarboximide (0.12 g, 0.316 mmol) was dissolved in 10 mL of DMF and added dropwise to the hot solution over the course of 1 h. The resulting solution was heated overnight under a nitrogen atmosphere. The DMF was then stripped, and the residue was taken up in methylene chloride and chromatographed on silica gel. Elution with 10% acetone in methylene chloride v/v yielded **12** as a yellow powder, 0.11 g, 50%. $C_{45}H_{41}N_5O_6$: mass spectrum (*m*/*e*) 746.9 (calcd 747.4), ^{1}H NMR (δ in $CDCl_3$) 8.76 (d, $J = 4.48$ Hz, 4H, naphthalene ring), 8.58 (d, $J = 7.33$ Hz, 1H, 8-naphthyl), 8.50 (d, $J = 8.1$ Hz, 1H, 2-naphthyl), 8.37 (d, $J = 8.2$ Hz, 1H, 6-naphthyl), 7.65 (d of d, $J = 8.4$ Hz, $J = 7.5$ Hz, 1H, 7-naphthyl), 7.16 (d, $J = 8.26$ Hz, 1H, 3-naphthyl), 6.69 (m, 2H, 4-phenyl, 6-phenyl), 6.54 (m, 1H, 2-phenyl), 4.18 (m, 2H, *N*-methylene), 3.22 (m, 4H, piperidine ring), 1.88 (m, 4H, piperidine ring), 1.7 (m, 2H, piperidine ring), 1.25 (broad singlet, 12H, octyl tail), 0.87 (t, $J = 4.0$ Hz, 3H, octyl tail methyl).

Compound 13. Compound **11** (0.412 g, 1.1 mmol) was dissolved in 20 mL of DMF and heated to 130°. *N*-(*n*-octyl)-benzene-1,2-dicarboxyanhydride-4,5-dicarboximide (0.358 g, 1.1 mmol) was dissolved in 15 mL of DMF and added dropwise to the hot solution over the course of 30 min. The reaction was heated under an atmosphere of nitrogen an additional 12 h. The solvent was stripped, and the resulting residue was taken up in a minimum amount of methylene chloride and precipitated by slowly dropping the methylene chloride solution into petroleum ether. The powdery precipitate was purified using silica gel column chromatography. Elution with 10% acetone in methylene chloride yielded **13** as a yellow powder (0.3 g, 39%). $C_{41}H_{39}N_5O_6$: mass spectrum (*m*/*e*) 698.9 (calcd 697.3), ^{1}H NMR (δ in $CDCl_3$) 8.458 (d, $J = 6.39$ Hz, 1H, 8-naphthyl), 8.381 (d, $J = 8.13$ Hz, 1H, 2-naphthyl), 8.279 (d, $J = 7.53$ Hz, 1H, 6-naphthyl), 8.184 (s, 2H, pyromellitimide), 7.549 (d of d, $J = 7.31$ Hz, $J = 8.3$ Hz, 1H, 7-naphthyl), 7.052 (d, $J = 8.14$ Hz, 1H, 3-naphthyl), 6.78 (t, $J = 1.93$ Hz, 1H, 2-phenyl), 6.731 (t, $J = 1.69$ Hz, 1H, 5-phenyl), 6.523 (t, $J = 1.87$ Hz, 1H, 4-phenyl), 3.9 (broad singlet, 2H, 5-phenylamine), 3.60 (t, $J = 7.33$ Hz, 2H, *N*-methylene), 3.115 (m, 4H, piperidine), 1.75 (m, 4H, piperidine), 1.58 (m, 2H, piperidine), 1.12 (broad singlet, 12H, octyl tail), 0.72 (t, $J = 4.15$ Hz, 3H, octyl tail methyl).

Compound 4. Compound **13** (0.126 g, 0.181 mmol) and *N*-(*n*-octyl)-naphthalene-1,8-dicarboxyanhydride-4,5-dicarboximide (0.07 g, 0.184 mmol) were dissolved in 10 mL of NMP. The solution was deoxygenated by bubbling with nitrogen and refluxed under a nitrogen atmosphere for 12 h. The reacted solution was taken up in 30 mL of chloroform and washed with 2 × 800 mL water. The chloroform solution was dried over anhydrous $MgSO_4$, and the chloroform was stripped on a rotary evaporator. The residue was chromatographed on silica gel, and elution with 5% acetone in methylene chloride v/v yielded **4** as a yellow powder, 0.052 g, 27%. $C_{63}H_{58}N_6O_{10}$: mass spectrum 1060.0 (calcd 1059.2), ^{1}H NMR (δ in $CDCl_3$) 8.815 (d of d, $J = 7.65$ Hz, $J = 7.62$ Hz, 4H, naphthalene ring), 8.64 (d, $J = 7.44$ Hz, 1H, 8-naphthyl), 8.56 (d, $J = 8.14$ Hz, 1H, 2-naphthyl), 8.49 (d, $J = 8.3$ Hz, 1H, 6-naphthyl), 8.38 (s, 2H, pyromellitimide), 7.914 (t, $J = 1.87$ Hz, 1H, phenyl ring), 7.86 (t, $J = 1.91$ Hz, 1H, phenyl ring), 7.73 (d of d, $J = 8.3$ Hz, $J = 8.42$ Hz, 1H, 7-naphthyl), 7.47 (t, $J = 1.83$ Hz, 1H, phenyl), 7.23 (d, $J = 8.4$ Hz, 1H, 3-naphthyl), 4.21 ($J = 7.4$ Hz, 2H, *N*-methylene), 3.75 (t, $J = 7.3$ Hz, 2H, *N*-methylene), 3.295 (m, 4H, piperidine), 1.93 (m, 4H, piperidine), 1.25 (broad singlet, 24H, octyl tails), 0.87 (m, 6H, octyl tail methyls).

Compound 5. Compounds **12** (0.071 g, 0.095 mmol) and **8** (0.124 g, 0.215 mmol) were dissolved in 5 mL of NMP and heated to 180° for 28 h under a nitrogen atmosphere. The solution was cooled, taken up in 30 mL of chloroform, and washed with water (2 × 1000 mL). The organic layer was dried over magnesium sulfate, and the solvent was stripped. The resulting residue was taken up in methylene chloride and adsorbed onto silica gel. Column chromatography and elution with 5% acetone in methylene chloride (v/v) gave **5** as a yellow powder, 30 mg, 24%. $C_{77}H_{62}N_8O_{14}$: mass spectrum (*m*/*e*) 1324.6 (calcd 1323.4), ^{1}H NMR (δ in $CDCl_3$) 8.825 (m, 8H, naphthalene rings), 8.65 (d, $J = 7.12$ Hz, 1H, 8-naphthyl), 8.58 (s, 2H, pyromellitimide ring), 8.57 (d, $J = 8.14$ Hz, 1H, 2-naphthyl), 8.44 (d, $J = 9.03$ Hz, 1H, 6-naphthyl), 7.95 (t, $J = 1.83$ Hz, 1H, phenyl spacer), 7.88 (t, $J = 1.87$, 1H, phenyl spacer), 7.72 (d of d, $J = 8.5$ Hz, $J = 7.85$ Hz, 1H, 7-naphthyl), 7.50 (t, $J = 1.83$ Hz, 1H, phenyl spacer), 7.215 (d, $J = 8.14$ Hz, 1H, 3-naphthyl), 4.21 (t, $J = 7.41$ Hz, 4H, *N*-methylenes), 3.26 (m, 4H, piperidine ring), 1.91 (m, 4H, piperidine ring), 1.76 (m, 2H, piperidine ring), 1.25 (broad singlet, 24 H, octyl tails), 0.88 (t, $J = 7.69$ Hz, 6H, octyl tail methyls).

Electrochemistry. Cyclic voltammetry was performed at a 25 μm Pt disk electrode in butyronitrile containing 0.2M tetra-*n*-butylammonium hexfluorophosphate. All measurements were made vs a Ag/Ag_xO reference electrode, while a Pt wire served as the counter electrode. Potentials were further referenced using a ferrocene internal standard.

Spectroscopy. UV−vis absorption measurements were made on a Shimadzu spectrometer (UV160). Steady state fluorescence measurements were made on a single photon counting fluorimeter (PTI). For fluorescence measurements the sample absorption at the excitation wavelength was kept within 5% of 0.1 to avoid reabsorption artifacts. The previously determined fluorescence quantum yield of ANI ($\Phi = 0.91$ in toluene[43]) was used as a standard for all quantum yield measurements.

The apparatus for nano- and microsecond transient absorption measurements has been described elsewhere.[43] Femtosecond transient absorption measurements were obtained with a pump wavelengths of 400 nm, 480 nm, or both using a Ti:sapphire laser system. A Spectra-Physics Millenium frequency-doubled CW Nd:YAG laser is used to pump a Coherent MIRA Ti:sapphire oscillator. The 107 fs fwhm laser pulses from the

oscillator are stretched to about 200 ps using a four-pass, reflective, single-grating pulse stretcher and are used to seed a homemade Ti:sapphire regenerative amplifier based on a 5 mm path length Ti:sapphire rod and a Medox two-step Pockels cell and driver. The amplifier is pumped by a homemade intracavity frequency-doubled (Type II LBO), Q-switched Nd:YAG laser (Quantronix 116E) operating at 2 kHz (3.5 mJ/pulse at 532 nm). The amplified Ti:sapphire pulse is recompressed to ~130 fs by a four-pass, reflective, single-grating pulse compressor. The pulse energy is ~350 μJ/pulse following compression. Four percent of the recompressed beam is split using a quartz disk, $\lambda/2$ waveplate−polarizer combination to adjust its intensity, and focused with a 100 mm focal length (fl) lens into a 2 mm thick sapphire disk. A stable white light continuum is generated by carefully adjusting the intensity of the pump beam to slightly above threshold. Continuum intensity fluctuations are typically under 5%. The white light beam is then split into probe and reference beams.

A second quartz disk is used to split off another 4% of the residual 800 nm light to generate another stable white light continuum pulse in the same manner as described above. This second white light pulse is used to seed a two stage optical parametric amplifier (OPA).[63] The remaining intense 800 nm beam is telescoped to a beam size of 1 mm and frequency doubled in a 2 mm thick type I LBO crystal, providing 110 μJ pulses at 400 nm. The 400 nm beam is split using a $\lambda/2$ waveplate−polarizer pair, with approximately 10 μJ diverted to pump the first stage of the OPA. The 400 nm beam and the white light continuum are focused with separate 30 mm fl lenses into a 2 mm type II β-Barium Borate (BBO) crystal. Spatial and temporal overlap of the beams is achieved by carefully adjusting a variable delay line and pointing of the beams. Energies of 0.3−0.4 μJ/pulse in the signal beam are achieved in the first stage. Amplification of parametric light from the first stage is achieved by overlapping the beam from the first stage with the remaining 95 μJ of 400 nm light in a 2 mm type I BBO crystal. The amplified parametric pulse (signal only, idler is rejected using cutoff filters) is typically 9−10 μJ/pulse, with a wavelength tuning range of 460−740 nm. The residual 400 nm light following parametric generation, about 20 μJ/pulse, is recollimated with a 500 mm fl lens. The parametric beam is collimated with a 400 mm fl lens and sent down a 1 m delay line which introduces a delay between it and the 400 nm beam. A dichroic mirror is used to spatially overlap the two pump beams before they are both sent down a 1.3 m variable delay line fitted with a retroreflector. Delays of 6 ns between the pump and probe are possible with 6.6 fs resolution.

For single pump excitation experiments the OPA beam is blocked and a mechanical chopper synchronized to one-half the repetition rate of the laser is used to block every other 400 nm pulse. However, when two pump pulses are used to excite the sample the first pulse occurs at 400 nm, and is not chopped. The second laser pulse is tuned to 480 nm and is chopped at one-half the repetition rate of the laser. This excitation scheme makes the probed absorption signal sensitive only to changes in state population induced by the second laser pulse.[39] The arrival time of the probe pulse is fixed, while the arrival of the two pump pulses can be varied relative to it and one another.

The pump beams are focused onto the sample using a 400 mm fl lens. The probe beam is focused separately using a 400 mm fl lens. The pump energies are attenuated using two $\lambda/2$ waveplate−polarizer combinations, one for each beam. Typical energies of each pump pulse are 1−1.5 μJ/pulse incident on the sample. The polarization of the pump beams are set at the magic angle (54.7°) with respect to the probe beam to avoid anisotropic effects. The probe and reference beams are vertically displaced, recollimated, and focused into a computer-controlled monochromator (SPEX 270M) with a 75 mm fl lens. The two beams are spatially separated after the exit slit and detected with matched silicon photodiodes. The amplifier outputs were measured with gated integrators and digitized with a 12 bit A/D board within a personal computer. The total instrument function is 180 fs.

Each shot pair (pump on, pump off) results in a single ΔA measurement. The reference pulse, in addition to being used for the ΔA calculation, is used to discriminate against probe pulses of abnormal intensity. Data sets are typically the average of 10 scans, with each point in the scan being an average of two hundred laser shots. Samples for the transient absorption experiments have optical densities at the excitation wavelength of ~0.5 (concentration $< 10^{-4}$ M) for 2 mm path length cells. Samples are stirred during the experiment using a wire stirrer, preventing thermal lensing and sample degradation.

Acknowledgment. This work was supported by the National Science Foundation (Grant CHE-9732840).

References and Notes

(1) Tajima, K. *Jpn. J. Appl. Phys.* **1993**, *32*, L1746-L1749.
(2) Nakamura, S.; Tajima, K.; Sugimoto, Y. *Appl. Phys. Lett.* **1994**, *65*, 283−285.
(3) Aviram, A.; Ratner, M. A. *Chem. Phys. Lett.* **1974**, *29*, 277−83.
(4) Hopfield, J. J.; Onuchic, J. N.; Beratan, D. N. *Science* **1988**, *241*, 817.
(5) Parthenopoulos, D. A.; Rentzepis, P. M. *Science* **1989**, *245*, 843−5.
(6) Garnier, F.; Horowitz, G.; Peng, X.; Fichou, D. *Adv. Mater.* **1990**, *2*, 592−4.
(7) Waldeck, D. H.; Beratan, D. N. *Science* **1993**, *261*, 576−7.
(8) Wagner, R. W.; Lindsey, J. S. *J. Am. Chem. Soc.* **1994**, *116*, 9759−60.
(9) Wagner, R. W.; Lindsey, J. S.; Seth, J.; Palaniappan, V.; Bocian, D. F. *J. Am. Chem. Soc.* **1996**, *118*, 3996−7.
(10) Willner, I.; Willner, B. *Adv. Mater.* **1997**, *9*, 351−355.
(11) Arrhenius, T. S.; Blanchard-Desce, M.; Dvolaitzky, M.; Lehn, J. M.; Malthete, J. *Proc. Natl. Acad. Sci. U.S.A.* **1986**, *83*, 5355−9.
(12) Carter, F. L. *Molecular Electronic Devices I*; Marcel Dekker: New York, 1982.
(13) Carter, F. L. *Molecular Electronics II*; Marcel Dekker: New York, 1987.
(14) Carter, F. L.; Siatkowski, R. E.; Wohltjen, H. *Molecular Electronic Devices*; North-Holland: Amsterdam, 1988.
(15) Pearson, D. L.; Schumm, J. S.; Tour, J. M. *Macromolecules* **1994**, *27*, 7, 2348−50.
(16) Tolbert, L. M. *Acc. Chem. Res.* **1992**, *25*, 561−8.
(17) DelMedico, A.; Fielder, S. S.; Lever, A. B. P.; Pietro, W. J. *Inorg. Chem.* **1995**, *34*, 1507−13.
(18) Birge, R. R. *Sci. Am.* **1995**, *272*, 90−5.
(19) Tamai, N.; Saika, T.; Shimidzu, T. *J. Phys. Chem.* **1996**, *100*, 4689.
(20) Kenny, P. W.; Miller, L. L. *J. Chem. Soc., Chem. Commun.* **1988**, 84.
(21) Huck, N. P. M.; Jager, W. F.; de Lang, B.; Feringa, B. L. *Science* **1996**, *273*, 1686−1688.
(22) Moerner, W. E.; Plakhotnik, T.; Irngartinger, T.; Croci, M.; Palm, V.; Wild, U. P. *J. Phys. Chem.* **1994**, *98*, 7382−9.
(23) O'Neil, M. P.; Niemczyk, M. P.; Svec, W. A.; Gosztola, D.; Gaines, G. L. I.; Wasielewski, M. R. *Science* **1992**, *257*, 63−5.
(24) de Silva, A. P.; Gunaratne, H. Q. N.; Gunnlaugsson, T.; Huxley, A. J. M.; McCoy, C. P.; Rademacher, J. T.; Rice, T. E. *Chem. Rev.* **1997**, *97*, 1515−1566.
(25) Archut, A.; Vogtle, F.; De Cola, L.; Azzellini, G. C.; Balzani, V.; Ramanujam, P. S.; Berg, R. H. *Chem. Eur. J.* **1998**, *4*, 699−706.
(26) Balzani, V.; Gomez-Lopez, M.; Stoddart, J. F. *Acc. Chem. Res.* **1998**, *31*, 405−414.
(27) Beyeler, A.; Belser, P.; De Cola, L. *Angew. Chem., Int. Ed. Engl.* **1998**, *36*, 22779-2781.
(28) Dickson, R. M.; Cubitt, A. B.; Tsien, R. Y.; Moerner, W. E. *Nature (London)* **1997**, *388*, 355−358.
(29) Feringa, B. L.; Huck, N. M. P.; Schoevars, A. M. *Adv. Mater.* **1996**, *8*, 681−684.

(30) Gobbi, L.; Seiler, P.; Diederich, F. *Angew. Chem., Int. Ed. Engl.* **1999**, *38*, 674−678.
(31) Gu, Z. Z.; Sato, O.; Iyoda, T.; Hashimoto, K.; Fujishima, A. *Chem. Mater.* **1997**, *9*, 1092−1097.
(32) Kulzer, F.; Matzke, R.; Braeuchle, C.; Basche, T. *J. Phys. Chem. A* **1999**, *103*, 2408−2411.
(33) Owrutsky, J. C.; Nelson, H. H.; Baronavski, A. P.; Kim, O. K.; Tsivgoulis, G. M.; Gilat, S. L.; Lehn, J. M. *Chem. Phys. Lett.* **1998**, *293*, 555−563.
(34) Schoevaars, A. M.; Kruizinga, W.; Zijlstra, R. W. J.; Veldman, N.; Spek, A. L.; Feringa, B. L. *J. Org. Chem.* **1997**, *62*, 4943−4948.
(35) Tsivgoulis, G. M.; Lehn, J. M. *Adv. Mater.* **1997**, *9*, 39−42.
(36) Weber, C.; Rustemeyer, F.; Duerr, H. *Adv. Mater.* **1998**, *10*, 1348−1351.
(37) Willner, I.; Doron, A.; Katz, E. *J. Phys. Org. Chem.* **1998**, *11*, 546−560.
(38) de Silva, A. P.; Gunaratne, H. Q. N.; Habib-Jiwan, J. L.; McCoy, C. P.; Rice, T. E.; Soumillion, J. P. *Angew. Chem., Int. Ed. Engl.* **1995**, *34*, 1728−1731.
(39) Debreczeny, M. P.; Svec, W. A.; Marsh, E. M.; Wasielewski, M. R. *J. Am. Chem. Soc.* **1996**, *118*, 8174−8175.
(40) Debreczeny, M. P.; Svec, W. A.; Wasielewski, M. R. *Science* **1996**, *274*, 584−587.
(41) Gosztola, D.; Niemczyk, M. P.; Wasielewski, M. R. *J. Am. Chem. Soc.* **1998**, *120*, 5118−5119.
(42) Feringa, B. L.; Schoevaars, A. M.; Jager, W. F.; De Lange, B.; Huck, N. P. M. *Enantiomer* **1996**, *1*, 325−335.
(43) Greenfield, S. R.; Svec, W. A.; Gosztola, D.; Wasielewski, M. R. *J. Am. Chem. Soc.* **1996**, *118*, 6767−6777.
(44) Debreczeny, M. P.; Svec, W. A.; Wasielewski, M. R. *New J. Chem.* **1996**, *20*, 815−828.
(45) Viehbeck, A.; Goldberg, M. J.; Kovac, C. A. *J. Electrochem. Soc.* **1990**, *137*, 1460−1466.
(46) Osuka, A.; Nagata, T.; Maruyama, K.; Mataga, N.; Asahi, T.; Yamazaki, I.; Nishimura, Y. *Chem. Phys. Lett.* **1991**, *185*, 88−94.
(47) Marcus, R. A. *J. Chem. Phys.* **1956**, *24*, 966.
(48) Wiederrecht, G. P.; Niemczyk, M. P.; Svec, W. A.; Wasielewski, M. R. *J. Am. Chem. Soc.* **1996**, *118*, 81−8.
(49) Ion pair distances were estimated from structures calculated using a modified MM2 force field and AM1 MO calculations performed within Hyperchem (Hypercube, Waterloo, Ontario).
(50) Fox, M. A. *Chem. Rev.* **1979**, *79*, 253−73.
(51) Scaiano, J. C.; Johnston, L. J.; McGimpsey, W. G.; Weir, D. *Acc. Chem. Res.* **1988**, *21*, 22.
(52) Eriksen, J. In *Photoinduced Electron Transfer*; Fox, M. A., Chanon, M., Eds.; Elsevier: Amsterdam, 1988; Vol. A, pp 391−408.
(53) Chervonnyi, V. S.; Sinyakov, G. N.; Gadonas, R.; Krasauskas, V.; Pelakauskas, A.; Maslov, V. G.; Prokof'eva, T. P. *Khim. Fiz.* **1990**, *9*, 340−6.
(54) Filatov, I. V.; Chirvonyi, V. S.; Sinyakov, G. N. *Opt. Spektrosk.* **1994**, *77*, 386-8.
(55) Filatov, I. V.; Chirvony, V. S.; Sinyakov, G. N. *Proc. SPIE−Int. Soc. Opt. Eng.* **1995**, *2370*, 95−8.
(56) Ishida, A.; Fukui, M.; Ogawa, H.; Tojo, S.; Majima, T.; Takamuku, S. *J. Phys. Chem.* **1995**, *99*, 10808−14.
(57) Fujita, M.; Ishida, A.; Majima, T.; Takamuku, S. *J. Phys. Chem.* **1996**, *100*, 5382−7.
(58) Majima, T.; Fukui, M.; Ishida, A.; Takamuku, S. *J. Phys. Chem.* **1996**, *100*, 8913−19.
(59) Gumy, J.-C.; Vauthey, E. *J. Phys. Chem. A* **1997**, *101*, 8575−8580.
(60) Cook, A. R.; Curtiss, L. A.; Miller, J. R. *J. Am. Chem. Soc.* **1997**, *119*, 5729−5734.
(61) Gosztola, D.; Wasielewski, M. R. Unpublished results.
(62) The first-order system of differential equations was solved using the fourth order Runge−Kutta method within Mathcad 7.0 Professional (MathSoft, Inc., USA).
(63) Greenfield, S. R.; Wasielewski, M. R. *Opt. Lett.* **1995**, *20*, 1394−6.